IBRACON Structures and Materials Journal
Revista IBRACON de Estruturas e Materiais
ISSN 1983-4195 ismj.org

ORIGINAL ARTICLE

Investigation of aggregate interlock contribution to shear strength of reinforced concrete and steel fiber reinforced concrete beams

Investigação da contribuição do engrenamento dos agregados em vigas de concreto armado e concreto reforçado com fibras de aço

Leticia Col Debella[a]
Luis Alberto Montoya-Coronado[b]
Thomás Lima de Resende[c]
Ricardo Pieralisi[d]

[a]Universidade Federal do Paraná – UFPR, Programa de Pós-graduação em Engenharia Civil – PPGEC, Curitiba, PR, Brasil
[b]Universidad de las Islas Baleares – UIB, Departamento de Ingenieria Industrial y de Construcción, Palma, España
[c]Universidade Federal dos Vales do Jequitinhonha e Mucuri – UFVJM, Instituto de Ciência, Engenharia e Tecnologia, Teófilo Otoni, MG, Brasil
[d]Universidade Federal do Paraná – UFPR, Centro de Estudos em Engenharia Civil – CESEC, Programa de Pós-graduação em Engenharia Civil (PPGEC), Curitiba, PR, Brasil

Received 20 September 2022
Accepted 31 March 2023

Abstract: Shear strength in reinforced concrete (RC) beams, especially in steel fiber reinforced concrete (SFRC) beams is a subject of great interest in structural engineering. In the case of beams without transverse reinforcement, the failure is explained based on a predefined crack pattern and kinematics, and the transfer of shear force accomplished through different mechanisms. Among these mechanisms, the aggregate interlock is present in most of the existing shear strength mechanical models in the literature, with divergences regarding its performance and preponderance. Thus, this paper focuses on evaluating the contribution of aggregate interlock throughout the critical crack formation process up to the ultimate load by performing bending tests on small-scale rectangular RC and SFRC beams without considering the effect of transverse reinforcement. The Digital Image Correlation (DIC) technique is used to track the patterns of shear cracks and their associated kinematics by measuring the relative displacements of opening (w) and sliding (δ). A detailed description of the shear behavior of these beams is provided by quantifying the aggregate interlock using the simplified Walraven model. The results help to understand the level of contribution of the aggregate interlock, and the main differences between structural elements of concrete with and without steel fibers in the scope of the shear strength.

Keywords: steel fiber reinforced concrete, aggregate interlock, shear.

Resumo: A resistência à força cortante em vigas de concreto armado (CA), especialmente em vigas de concreto reforçado com fibras de aço (CRFA), é um assunto de grande interesse na engenharia estrutural. No caso de vigas sem armadura transversal, a falha é explicada com base em um padrão de fissura pré-definido e sua cinemática, e a transferência da força cortante é feita por diferentes mecanismos. Dentre esses mecanismos, o engrenamento dos agregados está presente na maioria dos modelos existentes na literatura, havendo divergências quanto ao seu desempenho e preponderância. Assim, este trabalho se concentra em avaliar a contribuição do engrenamento dos agregados ao longo do processo de formação das fissuras críticas até a carga última, realizando ensaios de flexão em vigas retangulares de CA e CRFA de pequena escala sem levar em consideração o efeito da armadura transversal. A técnica de Correlação de Imagem Digital (CID) é usada para rastrear os padrões de fissuras de cisalhamento e suas cinemáticas associadas, medindo os deslocamentos relativos de abertura (w) e deslizamento (δ). Uma descrição detalhada do comportamento à força cortante dessas vigas é fornecida pela quantificação do engrenamento dos agregados, usando o modelo simplificado

Corresponding author: Leticia Col Debella. E-mail: leticiacoldebella@hotmail.com
Financial support: This study was financed in part by the Coordenação de Aperfeiçoamento de Pessoal de Nível Superior – Brasil (CAPES) – Finance Code 001, CNPq/MCTI/FNDCT Nº 18/2021 422189/2021-9; RTI2018-099091-B-C22 by 2 MCIN/AEI/10.13039/501100011033 and by "ERDF A way of making Europe"; and BIA2015-3 64672-C4-3-R (AEI – FEDER, UE).
Conflict of interest: Nothing to declare.
Data Availability: The data that support the findings of this study are available from the corresponding author, L. C. Debella, upon reasonable request.

de Walraven. Os resultados ajudam a entender o nível de contribuição do engrenamento dos agregados e as principais diferenças entre elementos estruturais de concreto com e sem fibras de aço no âmbito da força cortante

Palavras-chave: concreto reforçado com fibras de aço, engrenamento dos agregados, cisalhamento.

How to cite: L. C. Debella, L. A. Montoya-Coronado, T. L. Resende, and R. Pieralisi, "Investigation of aggregate interlock contribution to shear strength of reinforced concrete and steel fiber reinforced concrete beams" *Rev. IBRACON Estrut. Mater*., vol. 16, no. 3, e16303, 2023, https://doi.org/10.1590/S1983-41952023000300003

1 INTRODUCTION

The shear strength of reinforced concrete (RC) elements without transverse reinforcement may be resisted by different shear transfer actions that depend directly on the cracking pattern and its kinematics at the failure load [1]. During the shear failure process in beams without major arching effects, the shear transfer mechanisms that act are the residual stress; the dowel action; the height of the compressed zone; and the aggregate interlock [2].

Studies conducted by [3] and [4] have shown that the direct shear transfer capacity of cracked concrete in steel fiber reinforced concrete (SFRC) beams is significant with the use of fibers. However, there is currently no consensus among researchers regarding the development of critical cracks and activation of failure mechanisms during the process of crack formation leading up to the failure load for both traditional RC and SFRC [4], [5].

The aggregate interlock is one of the most controversial and debated shear transfer actions. Yang et al. [6] proposed a model where the aggregate interlock is the primary shear failure mechanism in conventional RC beams without transverse reinforcement. Other authors [7]–[11] have also suggested that the aggregate interlock plays a significant role in shear transfer. These authors have demonstrated that the mechanism represents a high percentage of shear in the failure process of RC elements, although its contribution may be variable.

In recent years, there have been differences among authors regarding the influence of aggregate interlock on the shear strength of SFRC. For example, in [4] and [12], the authors consider that aggregate interlock has an insignificant contribution to the shear strength. However, in [13] and [14] the authors state that the aggregate interlock is one of the most preponderant mechanisms in the failure of SFRC elements. The authors of [15] and [16] proposed a model that combines the aggregate interlock and pullout equations of steel fibers, claiming that it represents SFRC elements mechanically. Additionally, [17] demonstrates the influence of adding steel fibers to some aggregate interlock models.

This paper aims to evaluate the contribution of aggregate interlock in the process of critical crack formation up to failure load in both traditional RC and RC-SFRC beams. Flexural tests were conducted on small-scale rectangular beams without stirrups. Digital Image Correlation (DIC) technique was used to track critical shear cracking patterns and their associated kinematics throughout the experiment. Geometric characteristics, such as the shape and origin of the cracks, were identified [8]. The simplified Walraven's model [18] was employed to describe the behavior of aggregate interlock during the experimental test. The study provides a detailed understanding of the contribution of steel fibers in the behavior and mechanisms of shear transfer in SFRC structural elements.

2 SHEAR TRANSFER ACTIONS ON CONCRETE ELEMENTS

ACI-ASCE Committee 426 [19] identifies several mechanisms that may transmit internal forces between cracked sections in RC structures subjected to shear stresses. Figure 1 illustrates the main shear transfer actions: the vertical components of the residual stress (V_R); the uncracked compression zone (V_C); the aggregate interlock (V_{agg}); the dowel action (V_D); and, in the case of SFRC, the contribution of the steel fibers (V_F). Additionally, Figure 1 shows the arch action (V_{ARC}), which is related to the theoretical strut of the beam [20].

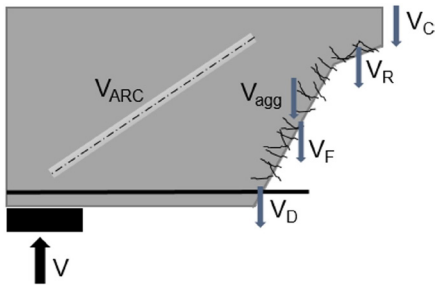

Figure 1. Shear transfer mechanisms in an SFRC beam

In SFRC beams, fibers provide additional tensile capacity along the crack [4], [13], [16]. In the compression zone of the cross-section, uncracked concrete provides shear strength. The residual stress capability comes from the aggregates, which allow the stress to be carried across the crack when the crack width opening (w) is small and there is no sliding (δ). The dowel action is the result of the interaction between the longitudinal rebars and the concrete that surrounds them, generating a sliding displacement (δ) in the fractured plane of the concrete [17]. The arch action of the theoretical strut assumes that no load is transferred through the cracks, and an inclined tension tie balances that shear forces. When the tensile strength of the concrete is reached in the tie, the bending crack propagates and the contribution of the strut is reduced [8], [9].

The aggregate interlock is a result of the contact forces between the aggregates that cross the critical shear crack, allowing the development of shear stresses due to the roughness of the cracked concrete [21]. In the case of the addition of steel fibers, the stress transfer bridge they provide may result in higher values of crack opening (w) and sliding (δ) compared to conventional concrete. This fact may lead to the overestimation of the level of contribution of aggregate interlock [15]–[17].

Walraven [18] proposed a theoretical model for the aggregate interlock shear transfer mechanism. The author approached the physical context of the aggregate interlock, which allowed for the relationship between the opening *(w)* and sliding *(δ)* between the cracked surfaces to the normal (σ) and tangential (τ) stresses transferred along critical cracks. The two-phase model (TPM) is mathematically complex, and its formulation makes it difficult to solve without numerical procedures. Therefore, Reinhardt and Walraven [22] proposed a simplified solution with linear equations as follows:

$$\sigma = -\frac{f_{cu}}{20} + [1.35w^{-0.63} + (0.19w^{-0.552} - 0.15)f_{cu}]\delta \quad (1)$$

$$\tau = -\frac{f_{cu}}{30} + [1.8w^{-0.8} + (0.234w^{-0.707} - 0.12)f_{cu}]\delta \quad (2)$$

where f_{cu} is the average compressive strength of cubic specimens (MPa), w is the crack width (mm) and δ is the crack sliding (mm).

The linear model equations were obtained by adapting the original model. This simplified model is limited by a maximum aggregate diameter (D_{max}) less than 32 mm and a compressive strength (f_{cu}) less than or equal to 59 MPa, both of which are met in the present study. In general, the original TPM model produces more stable results [15]–[17], [22] compared to the linear model, although the values are similar. Figure 2 shows the comparison between the two models, reiterating that, despite being more stable, the original TPM provides values close to the linear TPM. It should be noted that the work of Montoya-Coronado et al. [23] demonstrates that for low longitudinal reinforcement ratios (less than $\rho = 0.92$), the Walraven model overestimate the contribution of V_{agg}. This aspect was considered in this experimental campaign to ensure the accuracy of the results.

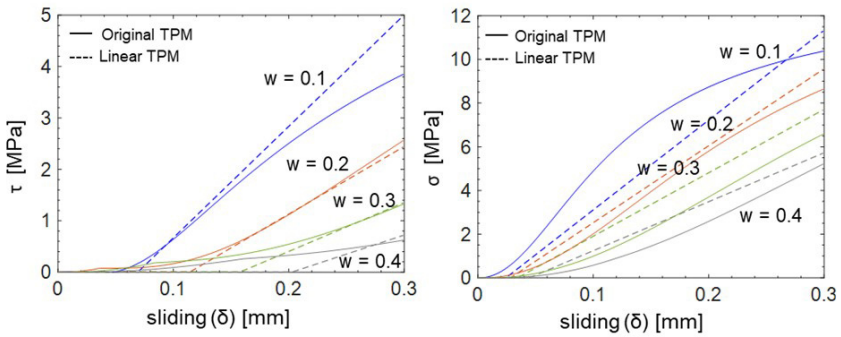

Figure 2. Sliding and opening obtained with the linear simplify TPM and the original TPM

3 CRITICAL SHEAR CRACKS KINEMATICS

Cavagnis et al. [8] employed Digital Image Correlation (DIC) to evaluate the shear transfer mechanisms in traditional RC beams without transverse reinforcement. The authors observed that the failure of the structural

components is closely related to kinematics of cracks, such as the appearance and propagation of critical cracks. Furthermore, Cavagnis et al. [8] noted that critical shear failure may be governed by different mechanisms for beams with similar characteristics, such as concrete dosage and beam geometry. These observations confirmed the conflicting ideas about the existing shear models, particularly the influence of the aggregate interlock contribution on shear strength. This mechanism is more affected by cracks kinematics than any other material characteristic or specificity [8].

Figure 3 illustrates the types of cracks that may appear during shear failure in RC beams under flexure test conditions [8], which can be categorized as follows:

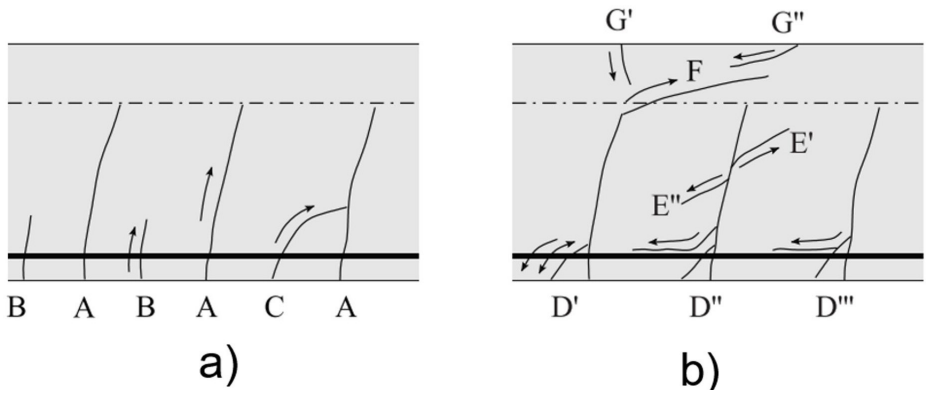

Figure 3. Types of cracks: (a) primary and secondary bending cracks; and (b) cracks caused by shear transfer actions. Source: Cavagnis et al. [8]

- Type A (Figure 2a): primary flexural cracks. These cracks arise from bending moments and typically one of them becomes the critical crack as the load increases.
- Type B (Figure 2a): secondary flexural cracks. These cracks occur between two primary flexural cracks or near the beam supports.
- Type C (Figure 2a): secondary or primary flexural cracks that merge with another primary flexural crack.
- Type D (Figure 2b): dowel cracks that develop at the same level of the flexural reinforcement. They typically join an inclined crack from the surface of the specimen to a primary flexural crack (type A) and often originate at low load levels.
- Type E (2-b): aggregate interlock induced cracks. These cracks form on either side of an existing crack and usually stem from primary or secondary bending cracks that transfer shear by aggregate interlock.
- Type F (Figure 2b): Propagation of a primary flexural crack within the compression zone. This occurs with a flat crack originating from a primary flexural crack, and usually happens at load levels near to failure.
- Type G (Figure 2b): Development of a crack within the compression zone not originating from a primary flexural crack. These cracks develop perpendicularly to the beam edge (G') due to the local bending of the compression chord, or at plane angles near to the load introduction region (G") due to the large shear forces in the compression zone and /or crushing of the compression chord.

4 EXPERIMENTAL PROGRAM

4.1 Specimens

Nine rectangular (10 x 20 cm) beams were produced, each with a length of 100 cm, resulting in an effective span of 90 cm. The beams were reinforced with rebars and steel fibers, except for three control beams that were only reinforced with rebars. The conventional reinforcement consisted of 2 bars with a diameter of 12.5 mm at the bottom (ρ = 1.25%) and 2 bars with a diameter of 8.0 mm at the top (ρ = 0.5%) of the section, all 4 arranged longitudinally. Additionally, 5.0 mm diameter stirrups were used every 60 mm in the transversal direction in the unmonitored half of the beam to ensure shear failure at other side of the beam (see Figure 4). The nominal concrete cover for the longitudinal and transversal reinforcement was 15 mm.

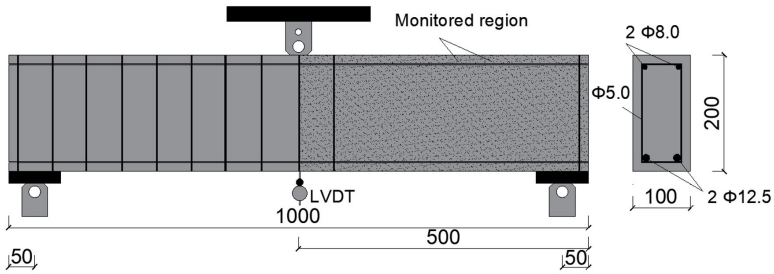

Figure 4. Conventional reinforcement of the beams (units in mm).

4.2 Materials and concrete compositions

A conventional concrete composition (C0) was prepared as a control for the RC beams, along with two SFRC compositions that varied in fiber content. Slightly adjustments were made to the proportion of material and super-plasticizer content to maintain consistency (slump of 100±10) in the fresh state mixes. The experimental program employed Cement type CPII F, natural sand, and basaltic coarse aggregate, with maximum diameter (D_{max}) of 12.7mm. The water-to-cement (w/c) was kept constant to ensure similar compressive strength. Hooked-end steel fiber contents of 0.5% (C0.5) and 1.0% (C1.0) in volume (40 kg/m3 and 80 kg/m3, respectively) were tested, and the primary fiber characteristics are shown in Table 1. In addition, super-plasticizer of type Muraplast FK 25 from MC-Bauchemie was used to reduce variations in the fresh-state properties of the concrete during the casting process. Table 2 summarizes the compositions used, along with the reference name assigned to each mix.

Table 1. Steel fiber characteristics

Dramix ® 3D 45/30 BL	
Length *lf* (mm)	30
Diameter *df* (mm)	0.62
Aspect ratio (*lf/df*)	45
Tensile strength *fy* (MPa)	1100
Nominal Young's modulus (GPa)	210
Nominal unit weight (g/cm^3)	7.85

Table 2. Characteristics of the concrete

Material	**C0**	**C0.5**	**C1.0**
Cement (kg/m^3)	468	468	468
Sand (kg/m^3)	684.9	684.9	684.9
Coarse aggregate (kg/m^3)	1013.9	1007.3	1000.6
w/c	0.45	0.45	0.45
Superplasticizer (kg/m^3)	0	1.04	1.08
Fiber volume (%)	0	0.5	1

The beams were cast by pouring concrete in accordance with EN 14651 [24], with the central increment being twice the lateral increments. Additionally, also following EN 14651 [24], the molds were filled up to 90% of the volume, and the remaining 10% were filled during vibration. The molds, filled with concrete, were vibrated externally to ensure uniform distribution. The beams were removed from the molds within 24 hours of casting, cured under a plastic sheet for 28 days, and then kept under laboratory conditions until the testing date. Prior to conducting the tests, the side face of the beam dimensioned to fail by shear was painted with a set of randomly spaced points (speckles) with adequate contrast to the surface. This painting is necessary to monitor the occurrence and propagation of cracks using the Digital Image Correlation (DIC) technique (for further details, refer to Section 4.3).

Moreover, for each composition, 8 cylindric samples (Φ100 x 200 mm) and 5 prismatic samples (150 x 150 x 550 mm) were cast to characterize the compressive (f_{cm}) (in accordance with NBR 5739: 2018 [25]) and flexural tensile strength ($f_{t,fl}$) (in accordance with NBR 16940:2021 [26]), respectively. The results of this characterization are presented in Table 3, with

the coefficient of variation of the tests in parentheses. Also in Table 3, f_{R1}, f_{R2}, f_{R3}, f_{R4} are the residual flexural strength referring to the crack openings of 0.5 mm, 1.5 mm, 2.5 mm, and 3.5 mm, respectively.

Table 3. Results of the characterization of concrete

		C0	C0.5	C1.0
Flexural Strength	f_{tfl} (MPa)	3.39 (10.7%)	4.02 (7.9%)	4.87 (12.5%)
	f_{R1} (MPa)	1.19 (22.3%)	3.29 (16.0%)	4.82 (13.1%)
	f_{R2} (MPa)	[-]	3.11 (17.8%)	4.25 (12.7%)
	f_{R3} (MPa)	[-]	2.72 (20.2%)	3.68 (10.3%)
	f_{R4} (MPa)	[-]	2.27 (18.2%)	3.03 (7.9%)
Compressive Strength	f_{cm} (MPa)	31.14 (4.3%)	35.56 (1.4%)	39.75 (4.3%)

4.3 Test setup

Flexural tests were conducted using an EMIC 23-300 Universal Testing System (from INSTRON®), which has a maximum capacity of 300 kN. The beams were simply supported by two steel roller supports, resulting in a theoretical shear span of 450 mm and the shear span to depth ratio (a/d) of 2.58. During the loading procedure, deflection at the center of the span was measured using a displacement transducer. The test was performed with displacement control at a rate of 0.02 mm/min, enabling a clear observation of crack development and propagation.

In addition, a Canon DSLR EOS Rebel SL3 camera equipped with an EF-S 40mm lens was used to record the test. The camera was placed perpendicular to the surface of the beam. The video was captured at 4 frames per second for each specimen, and a white light reflector was used during image capture to prevent shadows (see Figure 5). Boulekbache et al. [27] provide detailed information on the specimen preparation and DIC measurement technique for the test. The deformation and displacement fields were obtained using GOM Correlate software [28].

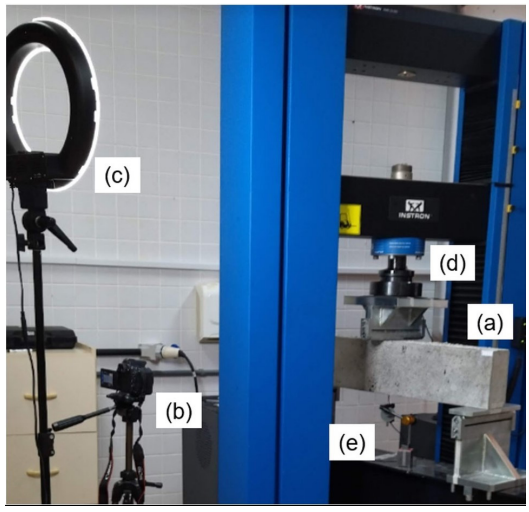

Figure 5. DIC test procedure. a) simply supported beam tested, b) Canon camera, c) light reflector, d) INSTRON press, e) LVDT

Figure 6 illustrates the crack discretization process used for measuring relative displacements (opening w and sliding δ) along the cracks (Figure 6a). Initially, each crack was divided into approximately 8 straight lines (Figure 6b). Each straight line was further subdivided into a set of segments with a length limited to the maximum diameter of the aggregate, as suggested by Cavagnis [9] (Figure 6c). The appropriate trigonometric manipulations of the horizontal and vertical measurements between the control points obtained throughout the experimental test were used to determine the relative displacements of crack opening (w) and sliding (δ). Figure 6 illustrates the crack discretization and the control points on both sides of the opening. Recently, Košćak *et al.* [29] and Assis et al. [30] presented a similar methodology and concluded that it was effective in measuring relative displacements.

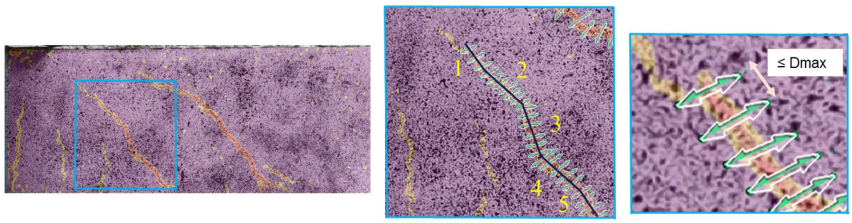

Figure 6. a) shear crack shown as major deformation in DIC, b) crack discretization and c) distance between segments limited by D_{max}

The values of w and δ were used in the Walraven aggregate interlock simplify model (Equation 1 and 2), and transformed into shear force (V_{agg}), as follows:

$$V_{\text{agg}} = b_w \left[\int_0^{lcr} \tau sen(\alpha) dl - \int_0^{lcr} \sigma \cos(\alpha)\, dl\right] \quad (3)$$

where b_w is the width of the beam, *lcr* is the total length of the analyzed critical crack, *dl* is the length for each segment, τ and σ are the tangential and normal stresses, respectively, from the Walraven equation (Equation 1 and 2), and α is the angle between the segment and the horizontal axis.

5 RESULTS AND DISCUSSIONS

The analysis of the results is organized in four subsections. The first three subsections describe the particularities observed during the initiation and propagation of cracks in individual tests carried out on RC beams without fiber reinforcement (C0), with a volume of 0.5% of fibers (C0.5) and with a volume of 1.0% of fibers (C1.0), respectively. The final subsection presents a comparison between all the results obtained.

5.1 Conventional concrete (C_0)

Figure 7 shows the shear forces versus mid-span deflection curve with the identification of the moments where cracks arose and the maximum load. The cracks are presented based on the description provided in section 3, with the flexural cracks indicated by the abbreviation FC.

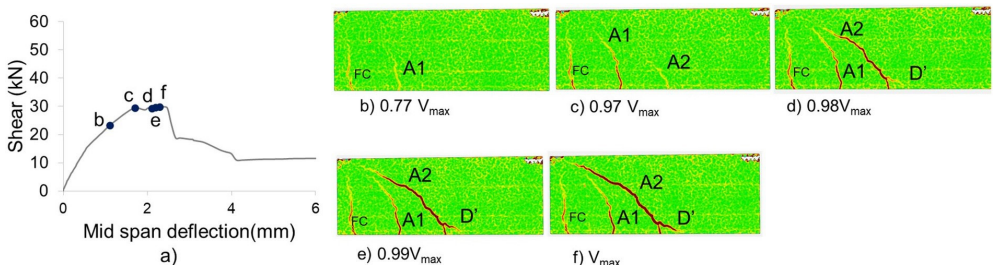

Figure 7. a) Shear force vs displacement curve, and cracking development of C_0 in b) 0.77V_{max}, c) 0.97V_{max}, d) 0.98V_{max}, e) 0.99V_{max}, and f) V_{max}

During the experimental test, at 77% of the maximum shear (Figure 7b), the first shear crack A1 appeared. From that moment on, the relative displacements of opening (w) and sliding (δ) were measured at A1. Later, at another point in time (Figure 7c), another inclined crack (A2) appeared at the longitudinal reinforcement height, and the relative displacements of opening (w) and sliding (δ) for the A2 crack were subsequently measured.

To understand the influence of the aggregate interlock on the cracking process, Figure 8 shows the development of this mechanism throughout the experimental test, measured for the two main critical shear cracks (A1 and A2). It is

important to note that the coordinate axis in Figure 8 represents the amount of the aggregate interlock expressed in terms of shear force for each instant of time in the experimental test. The abscissa axis represents the rate between the shear force at a given point and its maximum value, from beginning of the test to the failure load. The solid grey line represents the experimental shear force applied to the simply supported beams, presented as the applied force (V) divided by the maximum force resisted by the beam (V_{max}). In Figure 8, V represents the punctual shear, V_{agg} represents the shear force attributed to the aggregate interlock, and V_{crit} represents the shear force at which crack opening occurs.

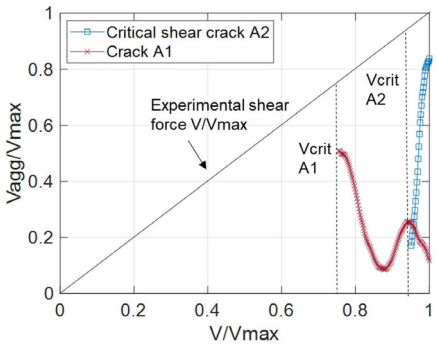

Figure 8. Aggregate interlock through the experimental test for cracks A1 and A2

In Figure 8, the blue curve represents the quantification of aggregate interlock on the critical crack (A2) throughout the experimental test. The A2 curve shows a significant increase in the contribution of aggregate interlock soon after its appearance, already at 97% of the maximum load V_{max}. The connection of a crack type D' with the critical crack triggers a larger opening w in this region, but there is no loss of the aggregate interlock mechanism due to the concomitant development of the crack towards the top of the beam, where the sliding (δ) continues to develop and transfer the aggregate interlock. Figure 9a shows the opening w, and Figure 9b shows the sliding (δ) at different times as a percentage of the maximum load V_{max}. An increase in sliding (δ) was observed in the steepest parts of the A2 crack, as mentioned, keeping the aggregate interlock contribution high. For a better understanding of the aggregate interlock curves, Figure 9 shows the opening and sliding of the two cracks (A1 and A2) throughout the evolution of the applied shear force, until the rupture in V_{max}.

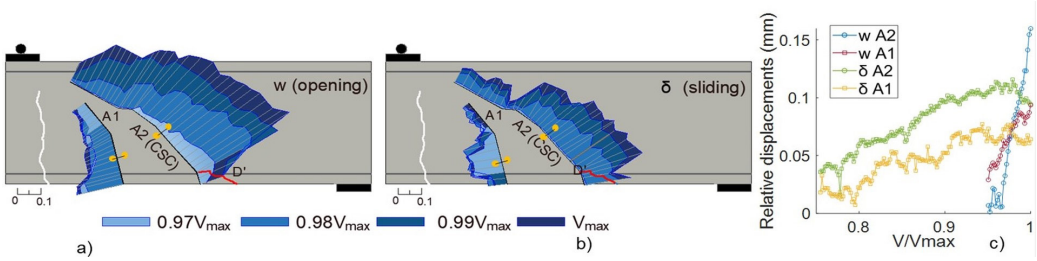

Figure 9. a) opening (w), b) sliding (δ) and c) relative displacements as a function of load variation for beam C_0

Concerning the first crack A1, the contribution of aggregate interlock showed a constant decline shortly after its appearance. Figure 9 depicts that the crack widened significantly more than the sliding throughout all the experimental test while the load increased up to failure. The primary reason for this is that the crack A1 remained nearly vertical.

It is important to note that opening *(w)* and sliding (δ) do not exhibit a fully ascending curve of values (Figure 9c). As cracks propagate, certain sections of these cracks may increase, decrease, or stabilize relative displacements. Depending on the current opening *(w)* and sliding (δ) combination, the aggregate interlock equation may transmit this phenomenon, oscillating between increasing and decreasing sections of the mechanism. Additionally, cracks initiate at one point and propagate towards the top surface of the beam. Thus, as the load progress, the crack propagates further, and more opening *(w)* and sliding (δ) measurements are taken. The variations in the aggregate interlock curves are a result of this variation since one section of the crack may have increasing opening development while another section

is still in its initial stages. The contribution of the aggregate interlock near the tensile reinforcement differs from that of the crack tip. Also, this variation may be due to redistribution and activation of other shear force transfer mechanisms.

The moment when the opening *(w)* of the critical crack A2 at 97% of the maximum load (Figure 7c) and the negligible contribution of the aggregate interlock of the crack A1 at practically the same instant indicate that another shear mechanism is responsible for transmitting the shear force on the beam. The works of Cavagnis et al. [8], and [30] suggest that, in shear failure, the load is initially resisted by mechanisms other than aggregate interlock. When the load application region is near the support, a secondary physical phenomenon, known as the arching action, can contribute to the direct transmission of loads to the support. For small values of a/d, cracks do not propagate through the inclined strut, and other shear modes such as shear-compression failure and arch action are observed. For larger values of a/d, flexure-shear cracks develop through the inclined struts, and a diagonal tension failure is observed. The shear span to depth ratio (a/d) influences the failure mode, as known from Kani's valley [32] and [33]. According to Kani [32], the limiting relationship can be a/d = 2.5. However, the author emphasizes that the a/d limit is not entirely decisive, and the mechanical behavior depends on other factors, such as the longitudinal reinforcement ratio.

When the theoretical compressed strut may develop undisturbed by the presence of a shear crack, the plastic shear strength solution may be applied. In such case, direct transmission occurs between the point of application and the support of the specimen. Figure 10 illustrates this phenomenon, where all the shear cracks emerge and propagate below a straight line connecting the load application point and the support, indicating that the theoretical strut has not been disturbed.

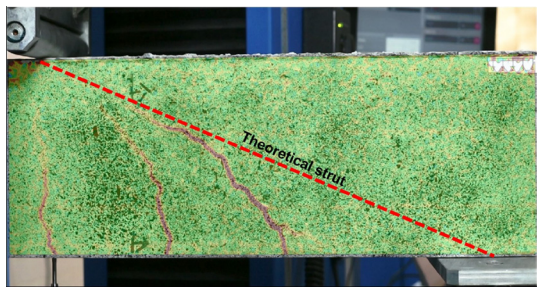

Figure 10. Theoretical strut developed without crack disturbances

Failure occurs when the critical crack crosses the theoretical strut (Figure 6e). In other words, the failure did not occur due to the loss of aggregate interlock linked to a larger crack opening, but rather due to the interruption of transmission by the compressed strut.

5.2 Concrete with 0.5% of steel fiber (C0.5)

Figure 11 illustrates the shear force versus mid-span deflection curve and the development of the cracking process for the beam made of concrete with a steel fiber content of 0.5% in volume (C0.5). Additionally, the flexural cracks that emerged in the middle of the beam span are identified as FC.

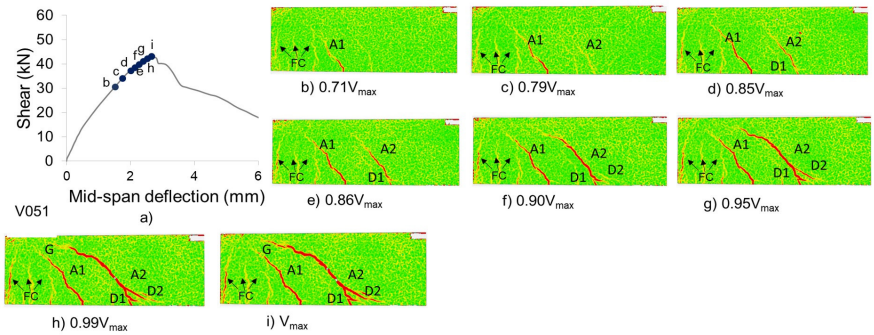

Figure 11. a) Shear force vs mid-span deflection curve, and cracking development of C0.5 in b) $0.71V_{max}$, c) $0.79V_{max}$, d) $0.85V_{max}$, e) $0.86V_{max}$, f) $0.9V_{max}$, g) $0.95V_{max}$, h) $0.99V_{max}$, i) V_{max}

Figure 11 illustrates the relative displacements measured for crack A1 from 71% of the maximum load V_{max} and for crack A2 from 79% of V_{max}, while Figure 12 shows the contribution of the aggregate interlock throughout the experimental test for both critical shear cracks.

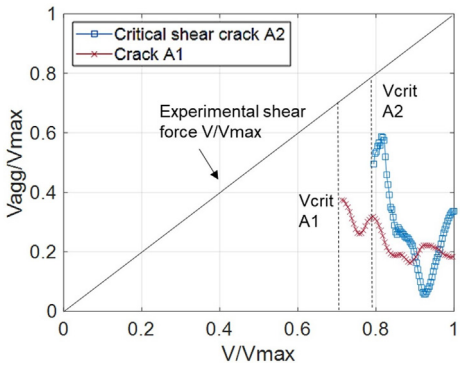

Figure 12. Aggregate interlock throughout the experimental test for the cracks A1 and A2

A D-type crack starts in the vicinity of A2 at 85% de V_{max} (Figure 11d), and soon after, at 86% de V_{max} (Figure 11e), joins A2. This union between D1 and A2 causes an increase in crack opening (w), resulting in a small drop in the contribution of the aggregate interlock, as shown in Figure 13b. This decrease in the contribution of the aggregate interlock due to the union between a type A and a type D crack was also observed in [8] and [31]. The phenomenon is repeated with the union of a new crack, D2, which joins A2 at 95% of V_{max}, again causing a sharp increase in opening (w) and consequently, loss of aggregate interlock. This drop can also be observed in Figure 13b, where the moment before and after the union of cracks A2 and D2 is detailed.

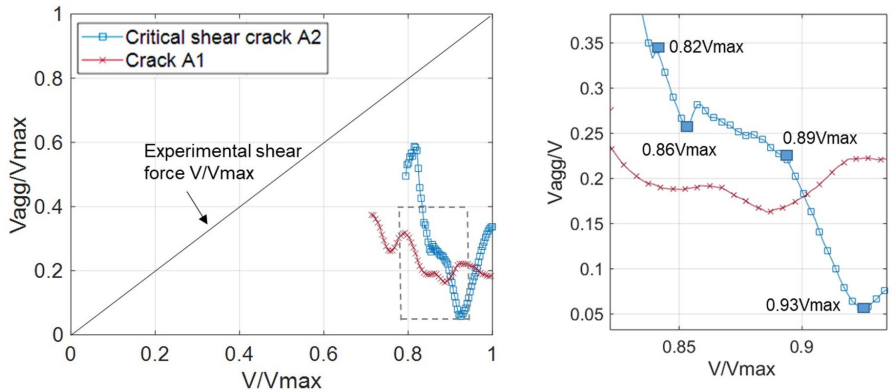

Figure 13. Decrease in the contribution of aggregate interlock due to the union of the crack D1 (0.82 and 0.86 of V_{max}) and D2 (0.89 and 0.93 of V_{max}) with A2

In Figure 11f, the almost horizontal portion develops in the A2 crack develops into a critical crack. The almost horizontal portion activates the residual stress mechanism of the concrete, which is characterized by pure tension without sliding (mode I), according to Yang et al. [6]. Figure 14b confirms that the sliding in the almost horizontal region of the A2 crack is very low, which is consistent with the literature. At this point, the residual stress becomes the main mechanism responsible for the transfer of shear force, with aggregate interlock present only in the steepest part of the crack where there is more sliding, as shown in Figure 14. These observations are consistent with those reported by Cavagnis et al. [8].

The variation of the aggregate interlock between higher and lower values, as shown in the Figure 12, follows the same reasoning presented for concrete C0. In other words, there is variation in both specific opening (w) and sliding (δ) measurements along the crack, where, as the load increases, more parts of the crack are activated.

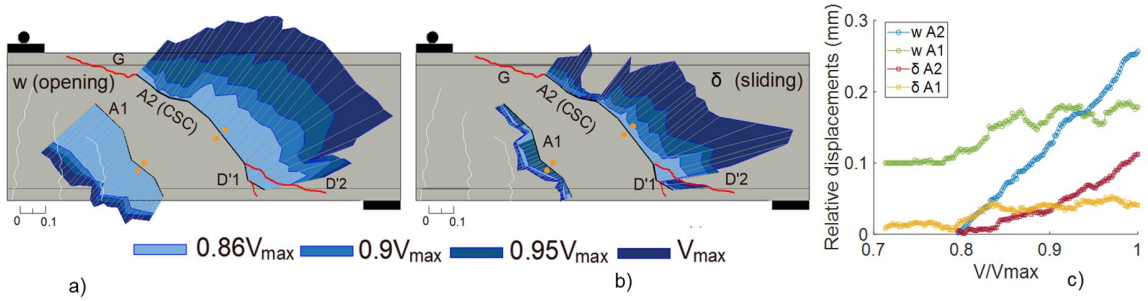

Figure 14. a) opening (w) b) sliding (δ) and c) relative displacements as a function of load variation for beam C0.5

The propagation of critical cracks is accompanied by the action of steel fibers, which act as a transfer bridge and regulate the crack opening, preventing brittle failure. This can be justified by observing the failure mechanism in the beams without fibers (C0) in the present work. With the predominant arching action, the shear cracks did not affect the compressed strut. Failure of the beams without fibers occurred when the compressed zone was crossed by the propagation of one of the main critical cracks, preventing the development of other shear transfer mechanisms due to the absence of large slidings (δ) and openings (w) associated with crack propagation.

After the union of crack D2 to A2, the aggregate interlock increases again from the steepest parts of the crack up to 0.99 of V_{max}. In fact, Figure 14 shows that even in the failure, there were significant values of crack opening *(w),* but there was also sliding (δ).

At 99% of failure (Figure 12h), a type G crack begins to propagate along the theoretical compressed strut due to the large shear forces in the compressed zone. At 99.9% of V_{max}, crack G merges with the critical crack leading to collapse. Figure 15 illustrates in detail the development of this crack G and its union with the critical crack.

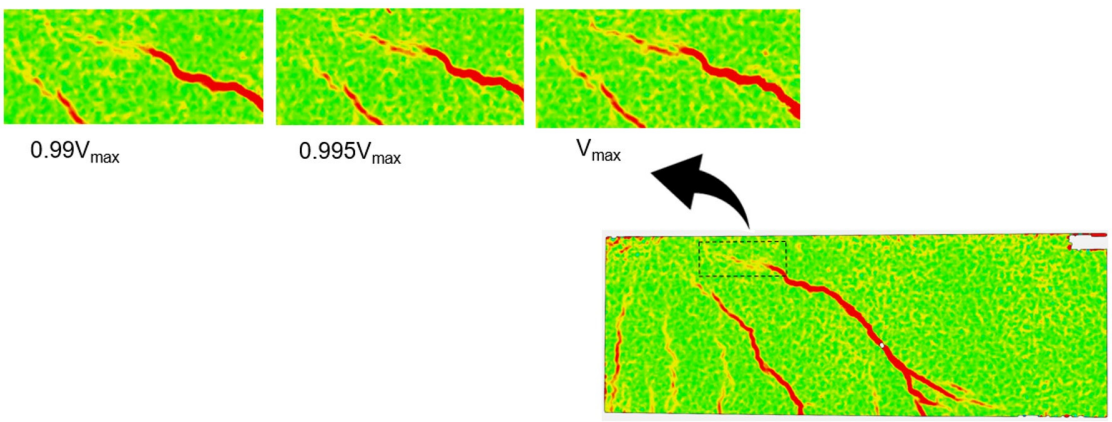

Figure 15. Type G crack developing in the compressed zone

At the tip of the critical crack between the initiation of the type G crack and the failure moment, the crack opening suddenly increased by approximately 30%, leading to a loss of the ability to transfer shear force through aggregate interlock. The specimen reached its maximum capacity when the aggregate interlock decreases due to the union of the critical crack A2 with the crack G of the compressed zone.

5.3 Concrete with 1.0% of steel fiber (C1.0)

For the beam with concrete containing 1.0% steel fibers (C1.0), the evolution of the cracking process, as well as its relationship with the shear force versus mid-span deflection curve, can be observed in Figure 16.

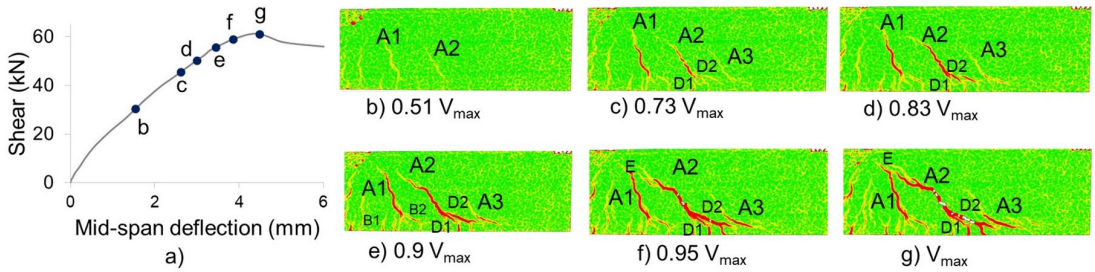

Figure 16. a) Shear force versus mid-span deflection, and cracking development of C1.0 in b) 0.51V_{max}, c) 0.73V_{max}, d) 0.83V_{max}, e) 0.9V_{max}, f) 0.95V_{max}, and g) V_{max}

The first two shear cracks (A1 and A2) appear at 51% of the maximum load. At 73% of V_{max} (Figure 16c), two doweling cracks (D1 and D2) appear and quickly join A2, causing a sharp increase in opening (*w*). A third flexural shear crack, A3, also appears. At 83% of V_{max} (Figure 16d), it can be observed that the A2 crack has developed to the point of being the critical shear crack, with its propagation going towards the upper surface of the beam. At 90% of the total loading (Figure 16e), in addition to the 3 shear cracks (A1, A2 and A3), type B secondary flexural cracks are also observed. In general, at this loading stage, a significant number of secondary bending cracks such as type B and C [8] can be seen appearing in the lower region of the beam, as shown in Figure 17. This fact is justified by the higher dosage of steel fibers in the composition, causing a constant redistribution of stresses in the specimen.

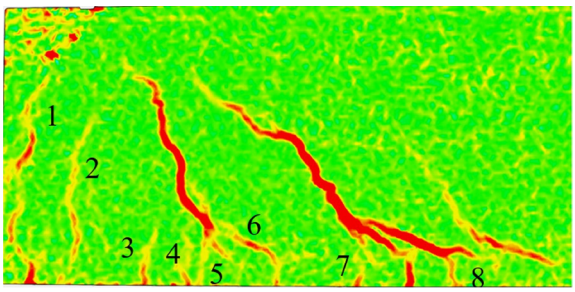

Figure 17. Secondary cracks in the C1.0 beam

At 95% of the maximum load (Figure 16f), a type E crack appears as a branch of the critical crack A2. This type of crack originates from the aggregate interlock, as presented in section 3. To understand the development of aggregate interlock in this beam, Figure 18 shows the simplified Walraven's model equation applied to the three cracks (A1, A2 and A3) during the experimental test.

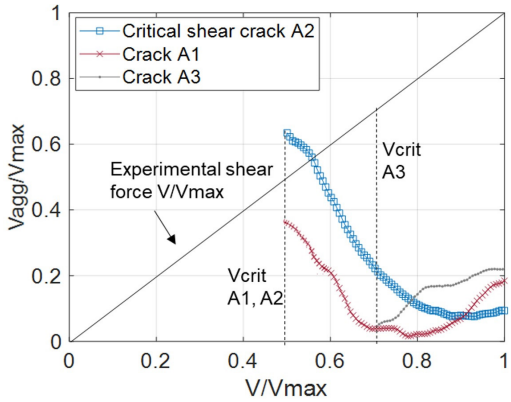

Figure 18. Aggregate interlock throughout the experimental test for cracks A1, A2 and A3

In Figure 18, it can be noted that the main crack (A2) shows a decreasing contribution from its appearance. The small contribution of the aggregate interlock in the main critical shear crack is mainly due to the predominance of the action of steel fibers. According to [15] and [16], the opening (w) in beams with fibers is usually larger than in conventional concrete, which reduces the friction within the crack, and consequently, the performance of the aggregate interlock.

In addition, the contribution of the aggregate interlock on shear strength could be overestimated when there is a no brittle failure as it is shown in Figure 18. This phenomenon can be explained due to high slippage to maintain equilibrium while cracks are forming. Furthermore, the steel fibers, which in this example have the highest dosage in the present experimental campaign, help to reduce the opening of cracks compared to the C0 reference beam. Thus, this issue is related to the sensitivity of the minimum crack opening accounted for in aggregate blocking contribution shear models at the beginning of the critical crack [23].

Figure 19 shows the opening w (Figure 19a) and sliding δ (Figure 19b) at the main test instants. The relative displacements of cracks A1 and A2 are also presented as a function of the load evolution (Figure 19c). It is clear that the opening (w) is greater than the sliding, supporting the hypothesis of little action of the aggregate interlock.

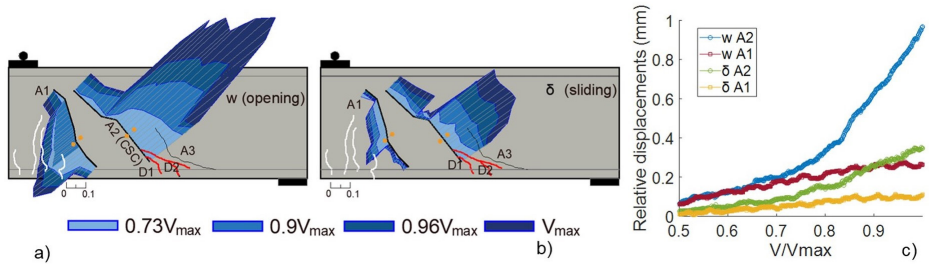

Figure 19. a) opening (w) b) sliding (δ) and c) relative displacements as a function of load variation for beam C1.0

Despite the larger opening in the critical crack, a type E crack emerged, theoretically designated to be the result of the action of the aggregate interlock [8]. In this case, the region where the crack emerged had a high sliding value δ, surpassing the opening w. The steeper and lower part of the crack had lost its contribution from the aggregate interlock due to the larger opening (w), but the crack tip region had more friction between the walls due to the high sliding (δ). Figure 20b shows a detailed view of the crack tip region at 95% of V_{max} (Figure 16f), where it can be observed in Figure 20a that the sliding δ was actually greater than the opening w. Failure occurred when the critical crack A2 gave rise to the crack E, which eventually merged with the crack A1. (Figure 16g).

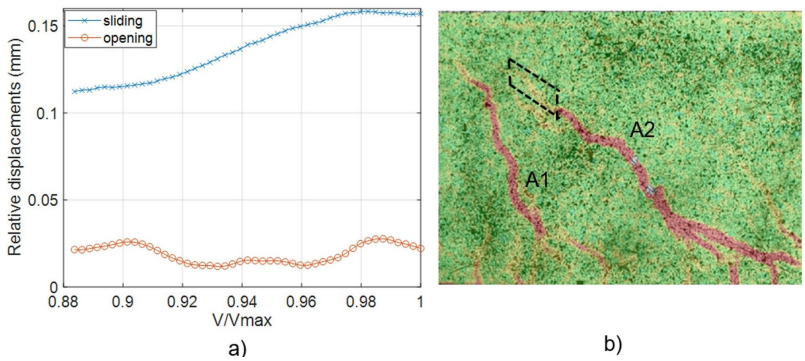

Figure 20. a) Opening (w) and sliding (δ) for the 88% to 95% of V_{max}, from the b) crack tip region

5.4 Comparison between the cases evaluated

To draw a comparison between the 3 evaluated beams, Figure 21 shows the measurement of a control point at of failure. The point was allocated to the steepest portion of each main crack (A2) and the measured opening is referred to as w_{max}, and the sliding as δ_{max}, as shown in Table 4.

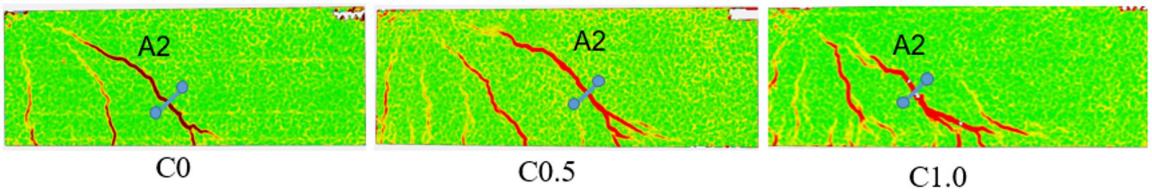

Figure 21. Control points measured at the failure

Table 4. Comparison between the beams.

	V_{max} (kN)	V_{crit}/V_{max}	w_{max} (mm)	δ_{max} (mm)	V_{agg_u}/V_{max}
C0	29.9	0.97	0.152	0.09	0.78
C0.5	43.3	0.79	0.249	0.11	0.34
C1.0	61.3	0.51	0.967	0.346	0.124

Table 4 provides a comparison of the shear forces resulting from the aggregate interlock at the failure (V_{agg_u}), as well as the maximum opening (w_{max}) and sliding (δ_{max}) for each of the three evaluated beams. As more fibers were incorporated into the concrete, the final opening w_{max} was observed to increase, consistent with findings from previous studies [4], [33] and [34]. In fact, the contribution of aggregate interlock was so low for concrete C1.0 that it was essentially negligible at just 12.4% of V_{max}. Conversely, for beam C0.5, aggregate interlock represented 34% of V_{max}.

Table 4 also displays the maximum crack opening for C1.0 concrete. Although this concrete type also experienced an increase in sliding, the considerably larger opening reduces the contribution of aggregate interlock.

Table 4 presents the critical shear value (V_{crit}) corresponding to the onset of the critical crack. By comparing the V_{crit}/V_{max} ratios, it is observed that the higher the fibers content in the concrete, the lower the V_{max} percentage at which the critical crack appears. This early initiation of the critical crack suggests that the FRC is better equipped to redistribute stresses in these elements. Conversely, in the case of C0 concrete without fibers, the critical crack emerged at 97% of the maximum load (V_{max}), propagating rapidly and leading to failure shortly after.

Finally, it is worth noting that the strength of the beams increased with the addition of steel fibers. According to the findings in [35], the proportion and characteristics of the steel fibers can influence the dosage required to effectively control cracking, increase the mechanical strength, and improve the ductility of the element. Specifically, volume contents ranging from 0.5% to 1.0% were found to be effective. In addition, [36] reported that the increase in shear capacity due to an increase in fiber volume depends on the a/d ratio. Specifically. the authors notated that for a/d =1, the shear strength increased by 96.6% when the fiber content was increased from 0% to 1.5%, while for a/d = 6, the shear strength increased by 32.2%. The authors also concluded that the fiber volume is a key variable affecting the shear strength of the elements. Nevertheless, there is no known proportional relationship since other factors, such as the a/d ratio, reinforcement ratio, and f_{cm}, can also influence the results.

5 CONCLUSIONS

The present study has evaluated the role of aggregate interlock in shear transfer in RC and SFRC beams using the simplified Walraven's model. DIC technique was employed to measure relative displacements at the cracks opening *(w)* and sliding *(δ)*. Based on the analysis of the experimental data, the following conclusions can be drawn:

- The simplified Walraven's equation was used to calculate the values of w and δ during the experimental test, up to failure. The results demonstrate that this equation accurately captures the phenomenon of aggregate interlock, although some overestimation of the calculated values was observed. Overall, the model provides a reliable representation of the mechanism under study.
- The influence of steel fibers on the mechanical behavior of the concrete was found to increase with the dosage used. In addition to enhancing the strength of the material, steel fibers caused a shift in the cracking pattern, due to their ability to redistribute stresses and alter the mechanisms of fracture in comparison to conventional concrete. As the volume of fibers in the mixture increases, the critical crack opening (w) also increases, leading to decrease in the contribution of aggregate interlock.
- The aggregate interlock plays a fundamental role in the failure process on SFRC beams. Observing the aggregate interlock during experimental tests helps to understand the activation of other shear resisting mechanisms. This fact

justifies exposing data throughout the beam failure process, rather than solely reading at the maximum load strength or the moment of failure.

- The evaluation of V_{crit} in the specimens indicated that the incorporation of more fibers into the concrete resulted in a lower relationship between V_{crit} and V_{max}. This observation supports the idea that fibers enable continuous stress redistribution, thereby promoting the development of the cracking process and activating more stress transfer mechanisms. In the case of C0 concrete, the critical crack occurred at a value very close to V_{max}. Although the aggregate interlock mechanism was not well developed, it proved to be the predominant mechanism in the failure process due to the limited crack opening.
- The C0 beams exhibited direct shear transmission to the support, which was primarily caused by the compressed strut related to Kani's valley phenomenon. Beams with fibers demonstrated a higher incidence of crack formation, resulting in a greater level of aggregate interlock.

Overall, the methodology presented herein provided to be effective in achieving its intended objectives. The test failure facilitated the assessment of aggregate interlock activation and development. Expanding the methodology to include other shear transfer mechanisms appears to be a rational approach for evaluating the individual contributions of each mechanism, particularly those of steel fibers.

ACKNOWLEDGEMENTS

The first author thanks CAPES and CNPQ for their financial support. All authors thank the PPGEC (Postgraduate Program in Civil Engineering) and CESEC (Centre for Civil Engineering Studies) at UFPR for their institutional support.

6 REFERENCES

[1] M. Tirassa, M. Fernández Ruiz, and A. Muttoni, "Influence of cracking and rough surface properties on the transfer of forces in cracked concrete," *Eng. Struct.*, vol. 225, pp. 111138, 2020.

[2] M. Fernández Ruiz, A. Muttoni, and J. Sagaseta, "Shear strength of concrete members without transverse reinforcement: a mechanical approach to consistently account for size and strain effects," *Eng. Struct.*, vol. 99, pp. 360–372, 2015.

[3] M. G. Cardoso, R. M. Lameiras, and V. M. S. Capuzzo, " Influence of concrete strength, fiber content, and aspect ratio in the residual flexural strength of steel fiber reinforced self-compacting concrete," *Rev. IBRACON Estrut. Mater.*, vol. 14, no. 5, e14503, 2021.

[4] M. R. Zarrinpour and S. H. Chao, "Shear strength enhancement mechanisms of steel fiber-reinforced concrete slender beams," *ACI Struct. J.*, vol. 114, no. 3, pp. 729–742, 2017.

[5] M. F. Ruiz and A. Muttoni, "Shear strength of members without transverse reinforcement as function of critical shear crack width," *ACI Struct. J.*, vol. 117, no. 1, pp. 103–118, 2020.

[6] Y. Yang, J. den Uijl, and J. Walraven, "Critical shear displacement theory: on the way to extending the scope of shear design and assessment for members without shear reinforcement," *Struct. Concr.*, vol. 17, no. 5, pp. 790–798, 2016.

[7] M. Classen, "Shear Crack Propagation Theory (SCPT): the mechanical solution to the riddle of shear in RC members without shear reinforcement," *Eng. Struct.*, vol. 210, pp. 110207, 2020.

[8] F. Cavagnis, M. Fernández Ruiz, and A. Muttoni, "Shear failures in reinforced concrete members without transverse reinforcement: An analysis of the critical shear crack development based on test results," *Eng. Struct.*, vol. 103, pp. 157–173, 2015.

[9] F. Cavagnis, "*Shear in reinforced concrete without transverse reinforcement: from refined experimental measurements to mechanical models*," Ph.D. dissertation, Ec. Polytech. Fed. Lausanne, Lausanne, 2017.

[10] M. Tirassa, M. Fernández Ruiz, and A. Muttoni, "Influence of cracking and rough surface properties on the transfer of forces in cracked concrete," *Eng. Struct.*, vol. 225, pp. 111138, 2020.

[11] M. Schmidt, P. Schmidt, S. Wanka, and M. Classen, "Shear response of members without shear reinforcement- experiments and analysis using shear crack propagation theory (SCPT)," *Appl. Sci. (Basel)*, vol. 11, no. 7, pp. 3078, 2021.

[12] A. Marì Bernat, N. Spinella, A. Recupero, and A. Cladera, "Mechanical model for the shear strength of steel fiber reinforced concrete (SFRC) beams without stirrups," *Mater. Struct.*, vol. 53, no. 2, pp. 28, 2020.

[13] S. Gali and K. V. L. Subramaniam, "Influence of cohesive stresses on shear capacity of reinforced SFRC beams without stirrups: A discrete crack approach," *Eng. Fract. Mech.*, vol. 206, pp. 218–232, 2019.

[14] T. Soetens and S. Matthys, "Shear-stress transfer across a crack in steel fibre-reinforced concrete," *Cement Concr. Compos.*, vol. 82, no. May, pp. 1–13, 2017.

[15] W. Kaufmann, A. Amin, A. Beck, and M. Lee, "Shear transfer across cracks in steel fibre reinforced concrete," *Eng. Struct.*, vol. 186, pp. 508–524, 2019.

[16] L. M. P. Matos, J. A. O. Barros, A. Ventura-Gouveia, and R. A. B. Calçada, "Constitutive model for fibre reinforced concrete by coupling the fibre and aggregate interlock resisting mechanisms," *Cement Concr. Compos.*, vol. 111, pp. 103618, 2020.

[17] T. L. Resende, D. C. Taissum Cardoso, and L. C. D. Shehata, "Experimental and theoretical investigation on the stress transfer across cracks due to combined action of steel fibers and aggregate interlock," *Cement Concr. Compos.*, vol. 124, pp. 104239, 2021.

[18] J. C. Walraven, "Fundamental analysis of aggregate interlock," *J. Struct. Div.*, vol. 107, no. 11, pp. 2245–2270, 1981, http://dx.doi.org/10.1061/JSDEAG.0005820.

[19] ACI-ASCE Committee 426, "The shear strength of reinforced concrete members," *J. Struct. Div.*, vol. 99, no. ST6, pp. 1091–1187, Jun 1973.

[20] A. Nouri et al., "Quantification of shear strength in reinforced concrete beams using digital image correlation: Experimental and analytical study," *Adv. Struct. Eng.*, vol. 24, no. 1, pp. 147–164, 2021.

[21] T. Huber, P. Huber, and J. Kollegger, "Influence of aggregate interlock on the shear resistance of reinforced concrete beams without stirrups," *Eng. Struct.*, vol. 186, pp. 26–42, 2019.

[22] H. W. Reinhardt and J. C. Walraven, "Cracks in concrete subject to shear," *J. Struct. Div.*, vol. 108, pp. 207–224, 1982.

[23] L. A. Montoya-Coronado, C. Ribas, J. G. Ruiz-Pinilla, and A. Cladera, "Time-history analysis of aggregate interlock in reinforced concrete beams without stirrups," *Eng. Struct.*, vol. 283, pp. 115912, 2023.

[24] International Union of Laboratories and Experts in Construction Materials, Systems and Structures, "Recommendations of RILEM TC 162-TDF: Test and design methods for steel fibre reinforced concrete Design of steel fibre reinforced concrete using the sigma-epsilon method: principles and applications," *Mater. Struct.*, vol. 35, no. 249, pp. 262–278, 2002.

[25] Associação Brasileira de Normas Técnicas, *Concreto – Ensaio de Compressão de Corpos de Prova Cilíndricos*, ABNT NBR 5739, 2018.

[26] Associação Brasileira de Normas Técnicas, *Concreto Reforçado com Fibras — Determinação das Resistências à Tração na Flexão (Limite de Proporcionalidade e Resistências Residuais) — Método de Ensaio*, ABNT NBR 16940, 2021.

[27] B. Boulekbache, M. Hamrat, M. Chemrouk, and S. Amziane, "Failure mechanism of fibre reinforced concrete under splitting test using digital image correlation," *Mater. Struct.*, vol. 48, no. 8, pp. 2713–2726, 2015.

[28] G. O. M. Aramis, *User Manual v6*. Braunschweig: GOM mbH, 2007.

[29] J. Košćak, D. Damjanović, M. Bartolac, and I. Duvnjak, "Shear behavior of RC beams without transverse reinforcement: An analysis of crack kinematics and transfer mechanisms based on stereophotogrammetric measurements," *Eng. Struct.*, vol. 255, pp. 2021, 2022.

[30] L. S. Assis, J. T. Assis, J. R. C. Pessoa, and A. D. Tavares Jr., "Elaboration of fracture prediction map using 2D digital image correlation - 2D CID," *Rev. IBRACON Estrut. Mater.*, vol. 15, no. 4, e15403, 2022.

[31] F. Cavagnis, M. Fernández Ruiz, and A. Muttoni, "A mechanical model for failures in shear of members without transverse reinforcement based on development of a critical shear crack," *Eng. Struct.*, vol. 157, pp. 300–315, 2018, http://dx.doi.org/10.1016/j.engstruct.2017.12.004.

[32] G. N. J. Kani, "Basic facts concerning shear failure," *ACI J. Proc.*, vol. 63, pp. 675–692, 1966.

[33] E. O. L. Lantsoght, "How do steel fibers improve the shear capacity of reinforced concrete beams without stirrups," *Compos., Part B Eng.*, vol. 175, pp. 107079, 2019.

[34] T. D. Dang, D. T. Tran, L. Nguyen-Minh, and A. Y. Nassif, "Shear resistant capacity of steel fibres reinforced concrete deep beams: An experimental investigation and a new prediction model," *Structures*, vol. 33, pp. 2284–2300, 2021.

[35] D. Carnovale and F. J. Vecchio, "Effect of fiber material and loading history on shear behavior of fiber-reinforced concrete," *ACI Struct. J.*, vol. 111, no. 5, pp. 1235–1244, 2014.

[36] S. A. Ashour, G. S. Hasanain, and F. F. Wafa, "Shear behavior of high-strength fiber reinforced concrete beams," *ACI Struct. J.*, vol. 89, no. 2, pp. 176–184, 1992.

Author contributions: LCD: writing, conceptualization, methodology, experimental program data curation, formal analysis, and paper review. LAMC: methodology, formal analysis, and paper review. TLR: methodology and formal analysis. RP: methodology, conceptualization, supervision, formal analysis, and paper review.

Editors: Leandro Trautwein, Mauro Real, Mario Pimentel.